



**HAL**  
open science

# Global spectral energy distribution of the Crab Nebula in the prospect of the Planck satellite polarisation calibration

J.F. Macias-Perez, F. Mayet, J. Aumont, F.X. Desert

► **To cite this version:**

J.F. Macias-Perez, F. Mayet, J. Aumont, F.X. Desert. Global spectral energy distribution of the Crab Nebula in the prospect of the Planck satellite polarisation calibration. *The Astrophysical Journal*, 2010, 711, pp.417-423. 10.1088/0004-637X/711/1/417 . in2p3-00232668v2

**HAL Id: in2p3-00232668**

**<https://hal.in2p3.fr/in2p3-00232668v2>**

Submitted on 4 Jan 2010

**HAL** is a multi-disciplinary open access archive for the deposit and dissemination of scientific research documents, whether they are published or not. The documents may come from teaching and research institutions in France or abroad, or from public or private research centers.

L'archive ouverte pluridisciplinaire **HAL**, est destinée au dépôt et à la diffusion de documents scientifiques de niveau recherche, publiés ou non, émanant des établissements d'enseignement et de recherche français ou étrangers, des laboratoires publics ou privés.

# Global spectral energy distribution of the Crab Nebula in the prospect of the Planck satellite polarisation calibration

J. F. Macías-Pérez, F. Mayet, J. Aumont

*LPSC, Université Joseph Fourier Grenoble 1, CNRS/IN2P3, Institut National Polytechnique de Grenoble, 53, av. des Martyrs, 38026 Grenoble, France*

F.-X. Désert

*Laboratoire d'Astrophysique, Obs. de Grenoble, BP 53, 38041 Grenoble Cedex 9, France*

## ABSTRACT

Within the framework of the Planck satellite polarisation calibration, we present a study of the Crab Nebula spectral energy distribution (SED) over more than 6 decades in frequency ranging from 1 to  $10^6$  GHz (from 299 to  $2.99 \times 10^{-4}$  mm). The Planck satellite mission observes the sky from 30 to 857 GHz (from 9.99 to 0.3498 mm) and therefore we focus on the millimetre region. We use radio and submillimetre data from the WMAP satellite between 23 and 94 GHz (from 13 to 3.18 mm) and from the Archeops balloon experiment between 143 (2.1 mm) and 545 GHz (0.55 mm), and a compendium of other Crab Nebula observations. The Crab SED is compared to models including three main components : synchrotron which is responsible for the emission at low and at high frequencies, dust which explains the excess of flux observed by the IRAS satellite and an extra component on the millimetre regime. From this analysis we conclude that the unpolarised emission of the Crab Nebula at microwave and millimetre wavelengths is the same synchrotron emission that the one observed in the radio domain. Therefore, we expect the millimetre emission of the Crab nebula to be polarised with the same degree of polarisation and orientation than the radio emission. We set upper limits on the possible errors induced by any millimetre extra component on the reconstruction of the degree and angle of polarisation at the percent level as a maximum. This result strongly supports the choice by the Planck collaboration of the Crab nebula emission for performing polarisation cross-checks in the range 30 (299 mm) to 353 GHz (0.849 mm).

*Subject headings:* Cosmic microwave background – Cosmology: observations, calibration

## 1. Introduction

As the strongest source of synchrotron radiation in our Galaxy, the pulsar-powered Crab nebula (*Taurus A*) is a well studied astrophysical object and it is therefore used for calibration purpose. This will be the case for the Planck satellite mission which will use the Crab Nebula for polarisation cross-checks in the frequency range from 30 to 353 GHz. A good understanding of the SED of the source as well as of the total intensity flux within the Planck beam will be required for an accurate determination of the angle of polarisation

of the detectors and of a possible cross polarisation effect between detector as they limit the accuracy to which the CMB polarised angular power spectra will be measured.

The emission spectrum of the A.D. 1054 supernova remnant has been the subject of a host of investigations over several decades in frequency. The radio spectrum is known to exhibit a synchrotron power law with a spectral index  $\beta \simeq -0.299 \pm 0.009$  (Baars *et al.* 1977). This continuum from radio synchrotron seems to be

fading with a rate  $\alpha = (-0.167 \pm 0.015)\%_{\text{yr}^{-1}}$  (Aller & Reynolds 1985). At higher frequency, above  $10^4$  GHz, the observations are also consistent with synchrotron emission with a power-law of spectral index  $-0.73$  (Veron-Cetty & Woltjer 1993). The data from IRAS satellite (Marsden *et al.* 1984) have been reanalyzed by (Strom & Greidanus 1992) revealing a significant excess of emission over the low frequency synchrotron spectrum, well explained by a single dust component at a temperature  $T \sim 46$  K, thus requiring a  $0.02 M_{\odot}$  dust mass. Using MPiFR bolometer arrays at the IRAM 30 m telescope, (Bandiera *et al.* 2002) gave the first evidence for a new component at millimetre wavelengths. They have shown that this 1.3 mm (230 GHz) excess flux cannot be interpreted as emission from a dust component whereas the data may be consistent with a low energy cutoff in the energy distribution of the emitting particles. However, at  $847\mu\text{m}$  (353 GHz) (Green *et al.* 2004) found a good agreement with the canonical radio synchrotron emission and hence no need for an extra component. As the Planck satellite mission will use the Crab nebula emission to perform polarisation cross-check in the range 30 to 353 GHz, a deep knowledge of the physical origin of this emission is needed.

For this purpose, we use observations of the Crab Nebula by the WMAP satellite at 23, 33, 41, 61 and 94 GHz (Page *et al.* 2007) and by the Archeops balloon experiment at 143, 217, 345 and 545 GHz (Macías-Pérez *et al.* 2007; Desert *et al.* 2008). These data in addition to already published data are used to study the Crab Nebula SED. The paper is organized as follows. In Sect. 2 we present the re-analysis of the Archeops and WMAP data. Sect. 3 presents the SED of the Crab Nebula from 1 to  $10^6$  GHz and compares it to a model including the synchrotron and dust well known components. In Sect. 4 we perform a coherent analysis of the Crab SED over the full frequency range adding an extra component to the previous model to account for the possible millimetre excess. The implications of our results for the Planck polarisation calibration are discussed in Sect. 5. Summary and conclusions are given in Sect. 6.

## 2. Re-analysis of the Archeops and WMAP observations

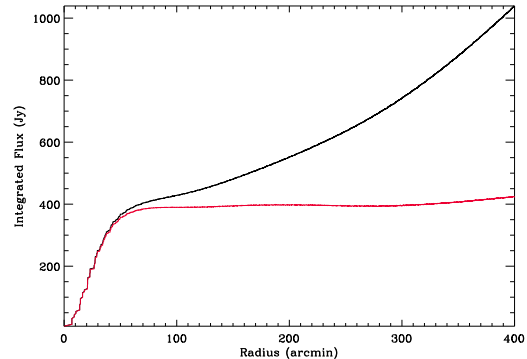


Fig. 1.— Integrated flux at 23 GHz as a function of the angular distance to the Crab nebula center before (black) and after (red) background subtraction.

In this paper we are mainly interested in the microwave and millimetre regime for which the best currently available data are the WMAP (Page *et al.* 2007) and Archeops (Desert *et al.* 2008) data. To avoid any bias on our analysis by a difference of treatment of these two data sets we have decided to re-estimate the Crab nebula unpolarised emission from 23 to 545 GHz using the publicly available WMAP (Page *et al.* 2007; Hinshaw *et al.* 2009) and Archeops (Macías-Pérez *et al.* 2007) intensity maps. Furthermore, to make the full data set as homogeneous as possible, the total intensity flux for each frequency was estimated using standard radial photometry techniques to mimic the flux integration performed for the high resolution data sets. Notice that we integrate far from the radio extension of the Crab nebula,  $\sim 5$  arcminutes radius, to recover the Crab nebula flux diluted over the entire beam pattern. Therefore, a key issue for this analysis is the subtraction of the background galactic emission which is mainly due to synchrotron and free-free emissions at low frequencies and dust at high frequencies. As the WMAP and Archeops maps are available on Healpix format we have developed our own radial photometry software for this pixelization scheme.

The results of this analysis are presented on ta-

ble 1. For Archeops we obtain similar values than those in (Desert *et al.* 2008) with slightly different error bars. However, for WMAP we obtain values 8 % larger than those in (Page *et al.* 2007). Most probably the difference comes from the way the background subtraction is performed and the fact the WMAP team computed the intensity and polarisation simultaneously. It is important to stress that the difference with respect to the WMAP team is within the  $1\text{-}\sigma$  error bars at high frequency and goes up to  $3\text{-}\sigma$  at 23 GHz. To illustrate the problem of background subtraction we show on figure 1 the radial profile centered at the Crab nebula position before (black) and after (red) background subtraction at 23 GHz. For this paper we use our own estimation of the Crab nebula flux in intensity but we have noticed that the final conclusions are not changed significantly by the choice of data set.

### 3. SED of the Crab Nebula

We present in this section a coherent analysis of the Crab SED in the range 1 to  $10^6$  GHz based on a compendium of observations shown in Table 1. Notice that to be able to directly compare to the Archeops and WMAP data, we have chosen only those data sets for which integrated fluxes over the full extension of the Crab Nebula are available.

#### 3.1. Low-frequency synchrotron emission

An accurate determination of the low-frequency synchrotron component is necessary to assess the synchrotron contribution at mm frequencies. Any inter-comparison of low-frequency radio observations of the Crab nebula must take into account its well-known secular decrease. In particular (Aller & Reynolds 1985) have estimated a secular decrease in the flux density at a rate  $\alpha = (-0.167 \pm 0.015) \%yr^{-1}$  from observations at 8 GHz over the period 1968 to 1984. This result is in good agreement with other studies at lower frequencies: for example  $\alpha = (-0.18 \pm 0.1) \%yr^{-1}$  over the period 1977 to 2000 at 927 MHz by (Vinyajkin 2005).

All these measurements are in fair agreement with theoretical evaluations of the evolution of pulsar driven supernova remnants by (Reynolds & Chevalier 1984) which predicts  $\alpha$  ranging from  $-0.16\%$  to  $-0.4\%yr^{-1}$ .

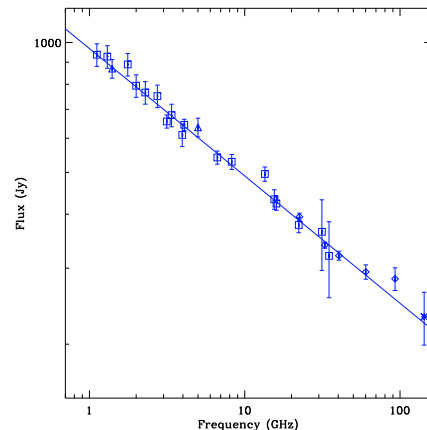


Fig. 2.— SED of the Crab Nebula from 1 to 100 GHz. Data samples are represented together with the best-fit power law model to the data (see text for details).

For this paper the value  $\alpha = -0.167 \%yr^{-1}$  is chosen for the fading of the Crab Nebula and all data are converted to a common observation date, 01/01/2003. In figure 2 we trace the flux of the Crab Nebula as a function of frequency for the fading corrected low-frequency data in table 1 ranging from 1 to 143 GHz.

We observe a large decrease of flux with increasing frequency which can be represented by a power law of the form  $A_1 \left(\frac{\nu}{1\text{GHz}}\right)^{\beta_1}$ . By  $\chi^2$  minimization, we obtain for the low-frequency data up to 100 GHz

$$\beta_1 = -0.296 \pm 0.006 \text{ and } A_1 = (973 \pm 19) \text{ Jy}$$

with  $\chi^2/N_{\text{dof}} = 1.03$  and this model is shown as a solid line on Fig 2. This result is in agreement with the "canonical" value  $\beta \simeq -0.299 \pm 0.009$  from (Baars *et al.* 1977)<sup>1</sup> at the  $1\text{-}\sigma$  level.

#### 3.2. High frequency synchrotron and dust emission

The Crab synchrotron emission described above evolves at higher frequencies, around  $10^4$  GHz, towards a much harder SED with a spectral index of  $\sim -0.73$  (see for example (Veron-Cetty & Woltjer 1993)). To accurately estimate the synchrotron emission

<sup>1</sup>(Kovalenko *et al.* 1994) obtained  $\beta_1 = (-0.27 \pm 0.04)$

| $\nu$ (GHz)         | $S_\nu$ (Jy) | $\Delta S_\nu$ (Jy) | Central Epoch | Reference                        |
|---------------------|--------------|---------------------|---------------|----------------------------------|
| 1.117               | 990.0        | 59.4                | 1969.9        | (Vinogradova <i>et al.</i> 1971) |
| 1.304               | 980.0        | 58.8                | 1969.9        | (Vinogradova <i>et al.</i> 1971) |
| 1.4                 | 930.0        | 46.5                | 1963          | (Kellermann <i>et al.</i> 1969)  |
| 1.765               | 940.0        | 56.4                | 1969.9        | (Vinogradova <i>et al.</i> 1971) |
| 2.0                 | 840.0        | 50.4                | 1969.3        | (Dmitrenko <i>et al.</i> 1970)   |
| 2.29                | 810.0        | 48.6                | 1969.3        | (Dmitrenko <i>et al.</i> 1970)   |
| 2.74                | 795.0        | 47.7                | 1969.3        | (Dmitrenko <i>et al.</i> 1970)   |
| 3.15                | 700.0        | 24.5                | 1964.4        | (Medd 1972)                      |
| 3.38                | 718.0        | 43.1                | 1969.3        | (Dmitrenko <i>et al.</i> 1970)   |
| 3.96                | 646.0        | 38.8                | 1969.3        | (Dmitrenko <i>et al.</i> 1970)   |
| 4.08                | 687.0        | 20.6                | 1964.8        | (Penzias & Wilson 1965)          |
| 5.0                 | 680          | 34                  | 1963          | (Kellermann <i>et al.</i> 1969)  |
| 6.66                | 577.2        | 20.2                | 1965.         | (Medd 1972)                      |
| 8.25                | 563.0        | 22.5                | 1965.9        | (Allen & Barrett 1967)           |
| 13.49               | 524.0        | 19.9                | 1969.9        | (Medd 1972)                      |
| 15.5                | 461          | 24                  | 1965.9        | (Allen & Barrett 1967)           |
| 16.0                | 447.0        | 15.6                | 1970.6        | (Wrixon <i>et al.</i> 1972)      |
| 22.285              | 397          | 16.0                | 1973.1        | (Janssen <i>et al.</i> 1974)     |
| 22.5                | 395          | 7                   | 2003          | <i>This paper</i>                |
| 31.41               | 387          | 72                  | 1966.7        | (Hobbs <i>et al.</i> 1968)       |
| 32.8                | 340          | 5                   | 2003          | <i>This paper</i>                |
| 34.9                | 340          | 68                  | 1967.3        | (Kalaghan & Wulfsberg 1967)      |
| 40.4                | 323          | 8.0                 | 2003          | <i>This paper</i>                |
| 60.2                | 294          | 10.0                | 2003          | <i>This paper</i>                |
| 92.9                | 285          | 16.0                | 2003          | <i>This paper</i>                |
| 111.1               | 290          | 35                  | 1973.5        | (Zablotnyi <i>et al.</i> 1976)   |
| 143                 | 231          | 32                  | 2002          | <i>This paper</i>                |
| 217                 | 182          | 38                  | 2002          | <i>This paper</i>                |
| 230                 | 260          | 52                  | 2000          | (Bandiera <i>et al.</i> 2002)    |
| 250                 | 204          | 32                  | 1985.3        | (Mezger <i>et al.</i> 1986)      |
| 300                 | 194.0        | 19.4                | 1983          | (Chini <i>et al.</i> 1984)       |
| 300                 | 131          | 42                  | 1978.75       | (Wright <i>et al.</i> 1979)      |
| 300                 | 300          | 80                  | 1976.0        | (Werner <i>et al.</i> 1977)      |
| 347                 | 190          | 19                  | 1999.8        | (Green <i>et al.</i> 2004)       |
| 353                 | 186          | 34                  | 2002          | <i>This paper</i>                |
| 545                 | 237          | 68                  | 2002          | <i>This paper</i>                |
| 750                 | 158          | 63                  | 1978.75       | (Wright <i>et al.</i> 1979)      |
| 1000                | 135          | 41                  | 1978.75       | (Wright <i>et al.</i> 1979)      |
| 3000                | 184          | 13                  | 1983.5        | (Strom & Greidanus 1992)         |
| 5000                | 210          | 8                   | 1983.5        | (Strom & Greidanus 1992)         |
| $12 \times 10^3$    | 67           | 4                   | 1983.5        | (Strom & Greidanus 1992)         |
| $25 \times 10^3$    | 37           | 1                   | 1983.5        | (Strom & Greidanus 1992)         |
| $3.246 \times 10^5$ | 6.57         | 0.66                | 1989          | (Veron-Cetty & Woltjer 1993)     |
| $4.651 \times 10^5$ | 4.78         | 0.48                | 1989          | (Veron-Cetty & Woltjer 1993)     |
| $5.593 \times 10^5$ | 4.23         | 0.42                | 1989          | (Veron-Cetty & Woltjer 1993)     |
| $7.878 \times 10^5$ | 3.22         | 0.32                | 1989          | (Veron-Cetty & Woltjer 1993)     |

Table 1: Compendium of Crab Nebula observations from 1 to  $10^6$  GHz. Fluxes ( $S_\nu$ ) are presented in Jy. For Veron-Cetty & Woltjer 1993 and Chini *et al.* 1984 a conservative 10% error has been chosen to account for extrapolation errors. The central epoch of observation is also indicated. This is used for the evaluation of the fading effect of the low frequency synchrotron component, up to 100 GHz. Data values labeled *This paper* for Archeops and WMAP are reevaluated using the method described in Section 2.

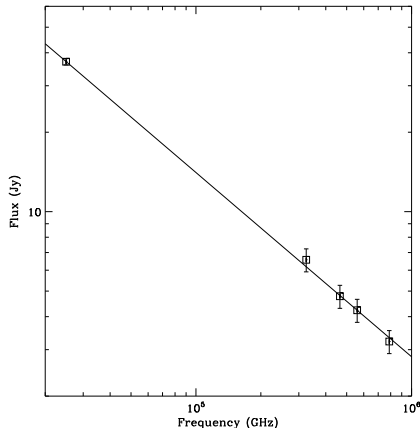


Fig. 3.— High frequency SED of the Crab Nebula. Data samples are represented together with the best-fit power law model to the data (see text for details).

properties at high frequency we have fitted the data from  $10^4$  to  $10^6$  GHz presented in table 1 to a power law of the form  $A_2\nu^{\beta_2}$ . By  $\chi^2$  minimization, we found the data to be well fitted,  $\chi^2/N_{\text{dof}} = 0.155$ , by a power law of parameters

$$\beta_2 = (-0.698 \pm 0.018) \text{ and } A_2 = (43.5 \pm 8.8) \times 10^3 \text{ Jy}$$

Figure 3 represents the high-frequency data and the best-fit power law model is overplotted.

Finally, the infrared satellite observatory IRAS has revealed significant excess emission above this synchrotron contribution around  $50 \mu\text{m}$  (Marsden *et al.* 1984). As shown by (Strom & Greidanus 1992) this can be explained, after careful removing of the synchrotron component, by a single dust component described by a modified black body of emissivity  $\beta = 2$  at  $T = 46 \pm 3$  K, requiring a dust mass of  $0.02 M_{\odot}$ .

### 3.3. Millimetric excess

To evaluate a possible millimetric excess of flux in the range 100 to 1000 GHz we assume the above canonical modeling of the Crab nebula SED: a synchrotron component with a spectral index break at high frequency and a dust component at infrared wavelengths. We can thus reconstruct the Crab nebula emission at the millimetric frequencies and

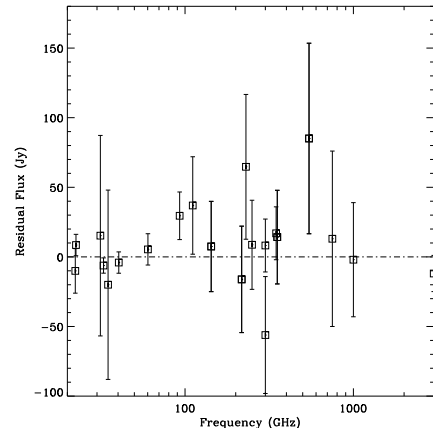


Fig. 4.— Residual to the standard model of the Crab nebula emission assuming a synchrotron and a dust component, in the range 10 to 2000 GHz (see text for details). Notice that the millimetric data were not used in the fit. We show the full data set in the region of interest.

compare it to the data in table 1. Fig 4 shows the residuals to the canonical model from 10 to  $2 \times 10^4$  GHz. We observe that there is no significant excess of power in the millimetric regime from 100 to 1000 GHz except for the 545 GHz Archeops data sample which presents only a 1.5 sigma excess. Indeed, the  $\chi^2/N_{\text{dof}}$  for the null hypothesis is 0.69.

## 4. Refined modeling

In the previous section we have proved that the millimetric data in table 1, from 100 to 1000 GHz, are compatible with the canonical model assuming single synchrotron and dust components. However, it is interesting to check if an extra component may improve significantly the fit to the data. Following (Bandiera *et al.* 2002) we consider either an extra low-temperature dust emission or an extra synchrotron component. Thus, the three component model is defined as follows

1. Canonical synchrotron that is described by four parameters: spectral index and amplitude for the low and high frequency emission. At high frequency we consider both the amplitude and the spectral index fixed and

set them to the values obtained in Sect. 3.2. At low frequency we fix the spectral index to the value obtained in Sect. 3.1 and the amplitude,  $A_S$ , is fitted. We also assume a constant fading of  $\alpha = -0.167 \text{ \%yr}^{-1}$  as before.

2. Canonical dust (following (Strom & Greidanus 1992)) described by a modified black body with three free parameters,  $A_D$ ,  $T_D$  and  $\beta_D$  that represent the amplitude, temperature and spectral index respectively.
3. One of the extra components as described below.

#### 4.1. Extra low-temperature dust emission

In Sect. 3.3 we concluded that at 545 GHz the difference between the standard model and the data is at its maximum. In the case of an extra dust component this implies very low temperature dust (LTD) in the range from 4 to 10 K. To model this component we assume a modified black body spectrum with three free parameters  $A_{LTD}$ ,  $T_{LTD}$  and  $\beta_{LTD}$  that represent the amplitude, temperature and spectral index respectively. The best-fit model to the data is found by  $\chi^2$  minimization on the full frequency range from 1 to  $10^6$  GHz.

Figure 5 presents on the left panel the observational data (black) and the global best-fit model to the data (in red). The canonical synchrotron component is shown on light blue and the canonical dust in orange. The extra low temperature dust component is represented in blue. The right panel presents the residuals to the best fit-model in the frequency range of interest. The parameters and error bars for the best-fit model to the data and the percentage of flux at 545 GHz associated to the extra component with respect to the total flux are given in table 2. We also present the  $\chi^2/N_{dof}$  values for the global fit in the frequency range from 1 to  $10^6$  GHz and on the millimetric range from 100 to 1000 GHz.

We obtain a good global fit to the data as shown by the  $\chi^2/N_{dof}$  value. The best-fit parameters obtained for the canonical synchrotron and dust components are in good agreement with those presented in Sect. 3. Comparing with

(Strom & Greidanus 1992), we found the same dust temperature,  $46 \pm 1$  K, with an error bar improved by a factor of three, as we carefully account for the canonical synchrotron spectrum. The amplitude of the extra component is compatible with zero and therefore we conclude that there are no evidence for an extra component in the form of low-temperature dust. Furthermore, we observe that on the one hand the data require extremely low temperatures of 5 K with rather large error bars, therefore dust masses of  $\sim 230 M_\odot$ , making the model rather unrealistic. On the other hand, the improvement of the  $\chi^2/N_{dof}$  in the millimetric region between 100 and 1000 GHz is not significant to justify the addition of the three extra parameters required by the low-temperature dust component. This is also clear on the right panel of figure 5 where we represent the residuals to the best-fit model to the data on the millimetric regime.

#### 4.2. Extra synchrotron component

For the extra synchrotron component we consider, as in (Bandiera *et al.* 2002), that the distribution of energy of the relativistic electrons responsible for the emission is well represented by a power law with spectral index in the range 1 to 3 and present a low-energy cutoff. To account for an excess of flux in the millimeter regime, the critical frequency corresponding to the lowest energy electrons must be somewhere in the range 200 to 600 GHz. In total the low-energy cutoff synchrotron (LECS) model has three parameters,  $p$  the spectral index of the electron energy distribution,  $\nu_c$  the low-energy cutoff critical frequency and  $A_{LECS}$ , a normalization coefficient. The best-fit to the data is found by  $\chi^2$  minimization.

The parameters and error bars of the best-fit to the data for the three data sets as well as the percentage of flux due to the extra component with respect to the total flux at 545 GHz are given on table 3. We also present  $\chi^2/N_{dof}$  values for the best-fit to the data on the full data set from 1 to  $10^6$  GHz and on the millimetric regime from 100 to 1000 GHz. The left panel of figure 6 presents the data in black and the global best-fit model to the data is represented in red. The canonical synchrotron component is shown on light blue and the canonical dust in orange. The extra low-energy

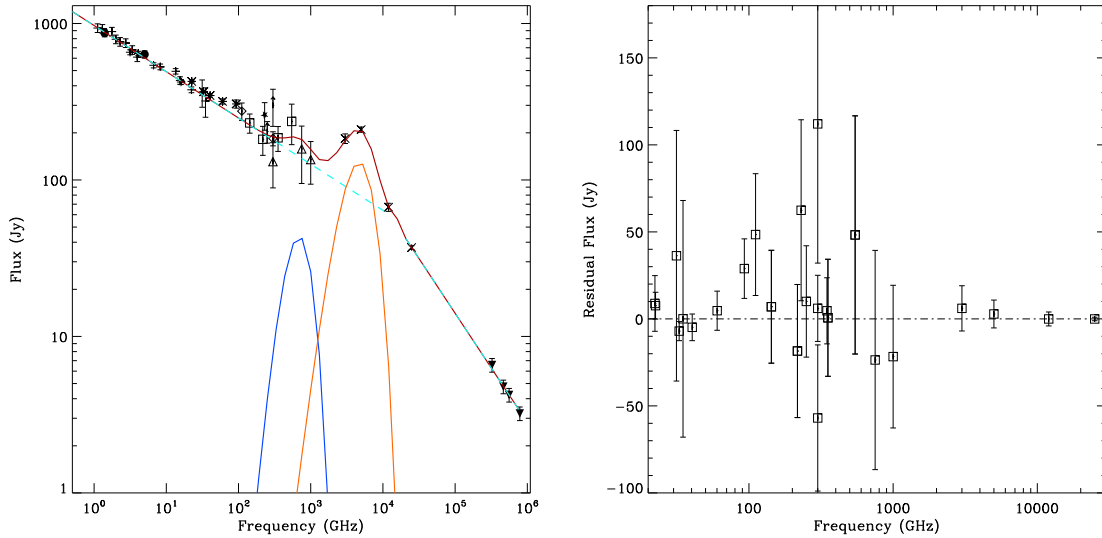


Fig. 5.— Refined modelling of the SED of the Crab nebula in the frequency range from 1 to  $10^6$  GHz assuming an extra dust component at low-temperature. Left panel: We represent the data from table 1 (black), the best-fit model to the data (red) and the synchrotron (light blue), the main dust (orange) and the extra dust (dark blue) components associated to it. Right panel: residuals in the millimetric regime for the top panel models.

| $\chi^2/N_{dof}$ | $A_s$ (Jy)  | $A_D$ (Jy)  | $T_D$ (K)      | $\beta_D$       | $A_{LTD}$ (Jy) | $T_{LTD}$ (K) | $\beta_{LTD}$ | LTD %       | $\chi^2_{mm}/N_{dof}$ |
|------------------|-------------|-------------|----------------|-----------------|----------------|---------------|---------------|-------------|-----------------------|
| 0.73             | $971 \pm 9$ | $128 \pm 8$ | $45.9 \pm 1.2$ | $1.93 \pm 0.50$ | $32 \pm 24$    | $5 \pm 23$    | $3.6 \pm 2.4$ | $26 \pm 20$ | 0.88                  |

Table 2: Best-fit model parameters and errors for the extra dust component model.  $\chi^2/N_{dof}$  for the full data set and on the millimetric regime from 100 to 1000 GHz. LTD % stands for the percentage of flux at 545 GHz due to the extra dust component with respect to the total flux.

| $\chi^2/N_{dof}$ | $A_s$ (Jy)   | $A_D$ (Jy)  | $T_D$ (K)      | $\beta_D$      | $A_{LECS}$ (Jy) | $\nu_c$ (GHz) | $p$        | LECS %    | $\chi^2_{mm}/N_{dof}$ |
|------------------|--------------|-------------|----------------|----------------|-----------------|---------------|------------|-----------|-----------------------|
| 0.76             | $965 \pm 14$ | $129 \pm 9$ | $46.0 \pm 1.0$ | $1.89 \pm 0.4$ | $5 \pm 6$       | $470 \pm 317$ | $3 \pm 12$ | $3 \pm 3$ | 0.93                  |

Table 3: Best-fit model parameters and errors for the extra synchrotron component model.  $\chi^2/N_{dof}$  for the full data set and on the millimetric regime from 100 to 1000 GHz. LECS % stands for the percentage of flux at 545 GHz due to the extra synchrotron component with respect to the total flux.

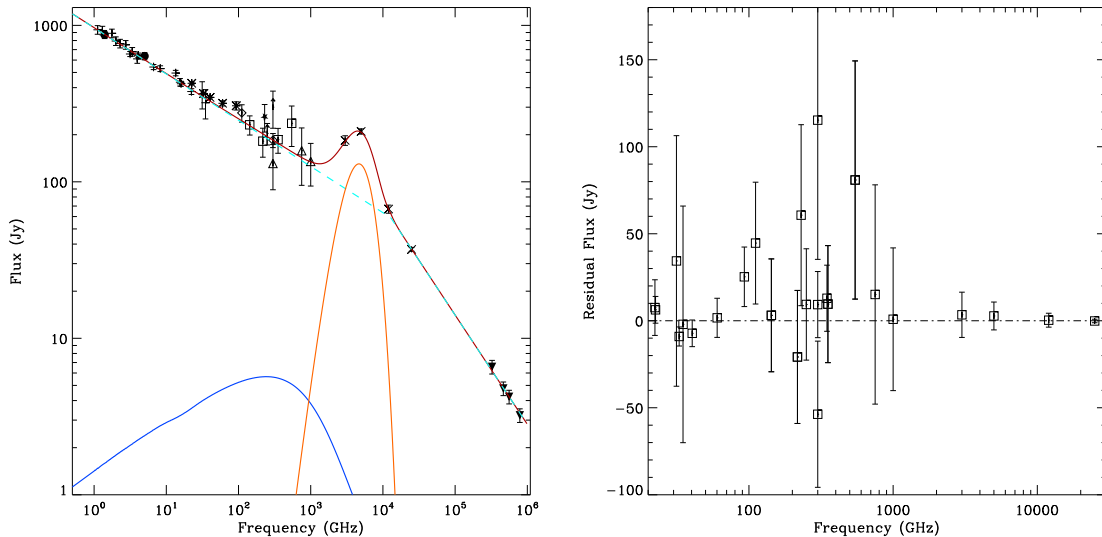


Fig. 6.— Refined modelling of the SED of the Crab nebula in the frequency range from 1 to  $10^6$  GHz assuming an extra synchrotron component. Left panel: We represent the data from table 1 (black), the best-fit model to the data (red) and the main synchrotron (light blue), the extra synchrotron (dark blue) and the dust components (orange) associated to it. Right panel: residuals in the millimetric regime for the top panel models.

cutoff synchrotron component is represented in blue.

As above, we obtain a good global fit to the data as shown by the  $\chi^2/N_{dof}$  value. The best-fit parameters obtained for the canonical synchrotron and dust components are in good agreement with those presented in Sect. 3 and on (Strom & Greidanus 1992). The amplitude of the extra synchrotron component is compatible with zero as well as the value of the spectral index of the electron energy distribution. We therefore conclude that there is no evidence of an extra component in the form of low-energy cutoff synchrotron. In addition, we observe that the  $\chi^2/N_{dof}$  in the millimetric region from 100 to 1000 GHz is worse than the one obtained in Sect 3.3 assuming the canonical model only. The right panel of figure 6 represents the residuals to the best-fit model to the data on the millimetric regime. From this we conclude that the fit to the data in this frequency regime is not improved by adding an extra synchrotron component.

We have also performed the analysis of the data set considering the  $p$  and  $\nu_c$  parameters fixed and set to the values quoted by (Bandiera *et al.* 2002). The analysis shows that the amplitude of the extra synchrotron component is compatible with zero and therefore we conclude that the data show no evidence of an extra synchrotron component.

## 5. Implications for the Planck satellite polarisation calibration

From the previous section, we conclude that the intensity emission of the Crab nebula at millimetre and submillimetre wavelengths is dominated by the well known synchrotron radiation observed at radio wavelengths. The data show no evidence of an extra synchrotron component and evidence for an extra dust component is not significant. Therefore, we can postulate that the Crab nebula emission at millimetre and submillimetre wavelengths is produced by the same relativistic electrons that the ones producing the radio emission. Then it is reasonable to guess that Crab nebula presents the same polarisation properties at radio

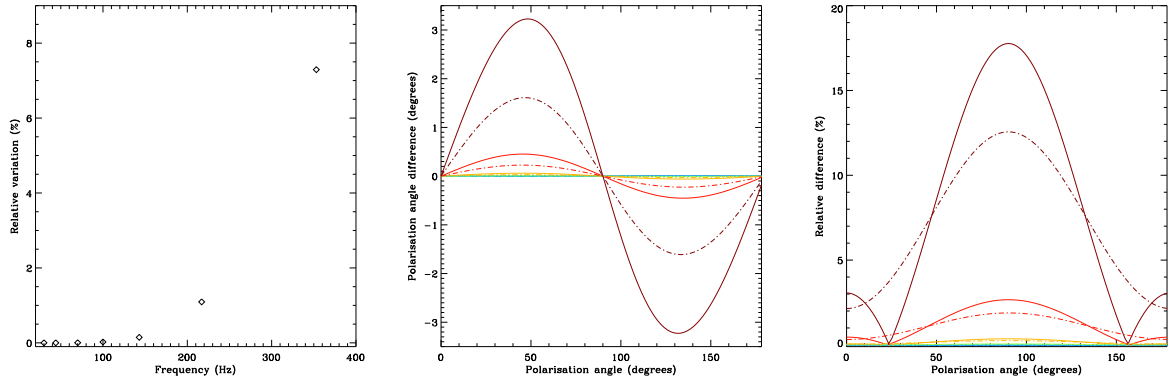


Fig. 7.— Errors induced in the degree and angle of polarisation by an extra low-temperature dust component. Left plot: relative error on the degree of polarisation on the case of an unpolarised extra component as a function of the frequency of the polarised Planck channels. Middle plot and right plot: relative error on the degree of polarisation and polarisation angle error on the case of an extra polarised component as a function of the polarisation angle of this component. The dashed and solid lines correspond to an extra component with a degree of polarisation of 5 % and 10 % respectively. From blue to red we represent the values for the different polarised Planck channels from 30 to 353 GHz.

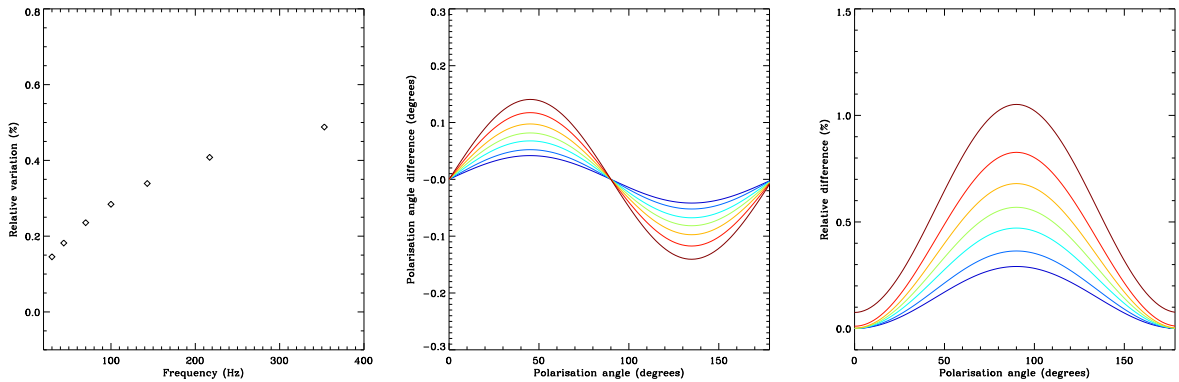


Fig. 8.— Errors induced in the degree and angle of polarisation by an extra low-energy cutoff synchrotron component. Left plot: relative error on the degree of polarisation on the case of an unpolarised extra component as a function of the frequency of the polarised Planck channels. Middle plot and right plot: relative error on the degree of polarisation and polarisation angle error on the case of an extra polarised component as a function of the polarisation angle of this component. From blue to red we represent the values for the different polarised Planck channels from 30 to 353 GHz.

and millimetre wavelengths. These conclusions are also supported by the Crab polarised emission observed from 23 to 94 GHz by the WMAP satellite (Page *et al.* 2007) when compared to the 363 GHz SCUBA measurements (Greaves *et al.* 2003) and the (Flett & Murray 1991) 273 GHz data. From these, it makes sense to use the low-frequency observations of the Crab nebula to cross-check and eventually update the knowledge of the polarisation characteristics of the high-frequency instruments as proposed by the Planck collaboration. As a summary and using the results from (Page *et al.* 2007; Greaves *et al.* 2003; Flett & Murray 1991) we expect the Crab nebula emission at the Planck frequencies to be polarised with a degree of polarisation of 8 to 9 % and a polarisation angle of  $150^\circ$  in equatorial coordinates (Aumont 2009). Then, at 30 GHz and 353 GHz we expect the total intensity to be  $351 \pm 7$  and  $173 \pm 5$  Jy and the polarised intensity about 28 and 15 Jy, respectively.

However, we can estimate upper limits on the errors induced on the determination of the degree of polarisation and polarisation angle of the Crab nebula emission at the Planck observation frequencies by the presence of an extra component. For this we use the results obtained on the previous section and we assume two different cases: polarised and unpolarised extra component. Figure 7 shows  $1-\sigma$  upper limits on the case of a low-temperature dust extra component. For the left plot we assume an unpolarised extra component and we present the error on the determination of the degree of polarisation as a function of the observation frequency. This error is below 1 % for the Planck CMB channels from 70 to 217 GHz and rise up to 8% at 353 GHz. The middle and right plot assume a polarised extra component and show the error on the polarisation angle and degree of polarisation, respectively, as a function of the polarisation angle of the extra component with respect to the main synchrotron component. From blue to red we show the errors from 30 to 353 GHz. The dotted-dashed and solid curve assume a degree of polarisation of 5 and 10 % for the extra component. As before the error on the degree of polarisation is below 1 % at the CMB channels and from 12 to 18 % at 353 GHz. For the polarisation angle the error is below  $0.2^\circ$  for the CMB

channels and at maximum of  $3^\circ$  at 353 GHz. Notice that the increase in the errors at 353 GHz is mainly due to the large value and large error bars of the Archeops data at 545 GHz and we do not think it is significant. Figure 8 shows the errors induced by an extra low-energy cutoff synchrotron component either unpolarised or polarised with a degree of polarisation equivalent to the one expected for the canonical synchrotron component. In this case the errors are much lower being well below 1 % and  $0.2^\circ$  for the degree and angle of polarisation, respectively, at all polarised Planck frequencies.

## 6. Summary and conclusions

Within the framework of the polarisation calibration of the Planck satellite emission we present in this paper a global analysis of the SED of the Crab Nebula in the frequency range from 1 to  $10^6$  GHz. For this purpose we have used new data from the WMAP satellite (Page *et al.* 2007) and from the Archeops balloon experiment (Desert *et al.* 2008) in addition to data currently available. We focus on the centimetric and millimetric regime as Planck observes the sky from 30 to 857 GHz.

We have first shown that the data are compatible with the canonical model of Crab nebula emission which assumes a synchrotron component at low and high frequencies, *plus* a dust component at the micrometre wavelengths. To check if an extra component may improve significantly the fit to the data, we consider either an extra low-temperature dust emission or an extra low-energy cutoff synchrotron component, as in (Bandiera *et al.* 2002). In both cases, we conclude that the current data present no evidence of an extra component. Therefore, the unpolarised millimetre flux of the Crab nebula is well represented by the following synchrotron power-law model

$$F_\nu = 973 \pm 19 \text{ Jy} \left( \frac{\nu}{1 \text{ GHz}} \right)^{(-0.296 \pm 0.006)} \exp(\alpha(T_{\text{obs}} - 2003)) \quad (1)$$

where  $\alpha = -1.67 \times 10^{-3} \text{ yr}^{-1}$  is the synchrotron fading and  $\nu$  and  $T_{\text{obs}}$  are the frequency and the date of observation in years A.C., respectively.

From above, we can conclude that the millimetre emission of the Crab nebula has the same phys-

ical origin than the radio synchrotron emission and therefore it is expected to be polarised with the same degree of polarisation and the same orientation. From the current data set we estimate that the errors on the reconstruction of the degree and angle of polarisation on the Planck cosmological channels induced by an extra component will be well below 1 %. This result strongly supports the choice by the Planck collaboration of the Crab nebula emission for performing polarisation cross-checks in the range 30 to 353 GHz (Aumont 2009).

We thank the Archeops collaboration for their efforts throughout the long campaigns. We acknowledge R. Bandiera and R.D. Davies for very helpful discussions. We finally thank Claudine Tur (LPSC) for fruitful help on bibliographic searches.

## REFERENCES

- Aller H. D. & Reynolds S. P., 1985, *ApJ*, 293, L73
- Allen R. J. & Barrett A. H., 1967, *ApJ*, 149, 1
- Aumont, J., 2009, *A&A*, submitted
- Baars J. W. M., Hartsuijker A. P. , 1972, *A&A*, 17, 172
- Baars J. W. M. *et al.*, 1977, *A&A*, 61, 99
- Bandiera R. *et al.*, 2002, *A&A*, 386, 1044
- Becklin E. E. & Kleinmann D. E., 1968, *ApJ*, 152, L25
- Chini R. *et al.*, 1984, *A&A*, 137, 117-127
- Dmitrenko T. *et al.*, 1970, *Radiofizika*, Vol. 13, No. 6, 823-829
- Desert F.-X., Macías-Pérez J. F. , Mayet F. *et al.*, 2008, *A&A*, 481, 411-421
- Flett, A. M. & Murray, A.G. 1991, *MNRAS*, 249, 4P
- Grasdalen G. L., 1979, *PACS*, 91, 436
- Greaves, J. S., Holland, W. S., Jenness, T., *et al.* 2003, *MNRAS*, 340, 353
- Hinshaw, B., *et al.*, 2009, *ApJ*, 180, 225-245
- Green D.A., Tuffs R.J. & Popescu C.C., 2004, *MNRAS*, 355, 1315-1326
- Hobbs R. W., Corbett H. H., Santini N. J., 1968, *ApJ*, 152, 43
- Janssen M. A., Golden L. M. and Welch W. J., 1974, *A&A*, 33, 373-377
- Kalaghan P. M. and Wulfsberg K. N., 1967, *Astronomical J.* , 72, 1051
- Kellermann K. I., Pauliny-Toth I. I. K., Williams P. J. S., 1969, *ApJ*, 157, 1
- Kovalenko A. V., Pynzar' A. V., Udaltsov V. A., 1994, *Astronomy Reports*, 38, 78-94
- Macías-Pérez J. F. *et al.*, 2007, *A&A*, 467, 1313
- Marsden P. L. *et al.*, 1984, *ApJ*, 278, L29

- Medd W. J., 1972, ApJ, 171, 41
- Mezger P. G. *et al.*, 1986, A&A, 167, 145
- Page, L. *et al.*, 2007, ApJ, 170, 335
- Penzias A. A. and Wilson R. W., 1965, ApJ, 142, 1149
- Reynolds S. P., Chevalier R. A., 1984, ApJ, 278, 630
- Strom R. G. & Greidanus H., 1992, Nature, 358, 654
- Véron-Cetty M. P. & Woltjer L., 1993, A&A, 270, 370
- Vinogradova L. V. *et al.*, 1971, Radiofizika, Vol. 14, No. 1, 157-159
- Vinyajkin E. N., 2005, astro-ph/0502033
- Werner M. W. *et al.*, 1977, PACS, 89, 127
- Wright E. L. *et al.*, 1979, Nature, 279,703
- Wrixon G. T. *et al.*, 1972, ApJ, 174, 399
- Zabolotnyi V. F., Kostenko V. I., Slysh V. I. 1976, Soviet Astronomy, 19, 405